POLITECNICO DI TORINO
Repository ISTITUZIONALE

Effect of annealing treatment and infill percentage on 3D-printed PEEK samples by Fused Filament Fabrication

Original
Effect of annealing treatment and infill percentage on 3D-printed PEEK samples by Fused Filament Fabrication / Lannunziata, E., Colucci, G., Minetola, P., Giubilini, A.. - In: INTERNATIONAL JOURNAL, ADVANCED MANUFACTURING TECHNOLOGY. - ISSN 0268-3768. - ELETTRONICO. - 131:(2024), pp. 5209-5222. [10.1007/s00170-024-13347-8]

Availability:
This version is available at: 11583/2986523 since: 2024-03-27T16:19:58Z

Publisher:
Springer

Published
DOI:10.1007/s00170-024-13347-8

Terms of use:

This article is made available under terms and conditions as specified in the corresponding bibliographic description in the repository

Publisher copyright

(Article begins on next page)

12 November 2026

The International Journal of Advanced Manufacturing Technology (2024) 131:5209–5222
https://doi.org/10.1007/s00170-024-13347-8

ORIGINAL ARTICLE

Effect of annealing treatment and infill percentage on 3D-printed PEEK samples by Fused Filament Fabrication

Erika Lannunziata[1,2] · Giovanna Colucci[2,3] · Paolo Minetola[1,2] · Alberto Giubilini[1,2]

Received: 1 December 2023 / Accepted: 22 February 2024 / Published online: 2 March 2024
© The Author(s) 2024

Abstract

A strategy that is gaining momentum in several industrial sectors is metal replacement, which aims to find suitable alternatives for replacing metal components with lighter ones. One possible solution is represented by high-performance polymers (HPP), which are a family of materials with improved thermo-mechanical and functional properties, compared to commodity plastics. Additive manufacturing (AM) is revolutionizing the industrial world due to its high design freedom, dimensional accuracy, and shortened total production time. Thus, combining the use of HPP with AM technologies could lead to innovative results, which could offer new metal replacement solutions through redesign and new material properties. However, HPPs have some manufacturing limitations, for example, they require high processing temperatures, and some of them are subject to significant warping and deformation phenomena. This aspect is particularly significant for semi-crystalline polymers, as in the case of poly(ether-ether-ketone) (PEEK), which is affected by thermal gradients during 3D printing. In this research, an investigation was carried out on the Fused Filament Fabrication (FFF) of different 3D printed PEEK samples, evaluating the effect on final properties not only of various infill percentages (30%, 50%, 70%, and 100%) but also of two different heating treatments. In this regard, a traditional annealing in oven, post 3D printing, was compared to a direct annealing approach, performed during FFF. The mechanical performance of the samples was characterized through tensile and compression tests along with the thermal properties and the thermal stability. In addition, for all different cases, energy consumption was measured, to provide an indication of the sustainability of the presented approaches. The findings suggest that the direct annealing solution holds promise and merits further investigation to bridge knowledge gaps in this domain. This research contributed to advance the understanding of PEEK 3D printing by FFF and played a vital role in the practical implementation of metal replacement as a sustainable strategy across various industrial applications.

Keywords High-performance polymers · Poly(ether-ether-ketone) · Additive manufacturing · Fused filament fabrication · Heat treatment · Direct annealing

1 Introduction

Metal replacement is an approach that deals with finding suitable alternatives to commonly produced metal components, introducing some interesting advantages, such as weight reduction, shortening processing cycles, lowering shipping costs, and reducing vibration and noise [1]. When metal replacement started, it was mainly focused on large-scale consumer goods, and plastic was a valid substitute, due to its lower cost. However, for some industrial applications, substituting metals with polymers was a huge challenge, due to the lower mechanical properties of common polymers [2]. Nowadays, the widespread of high-performance polymers (HPP) led to the replacement

✉ Alberto Giubilini
alberto.giubilini@polito.it

[1] Department of Management and Production Engineering (DIGEP), Politecnico Di Torino, Corso Duca Degli Abruzzi 24, 10129 Turin, Italy

[2] Integrated Additive Manufacturing Centre (IAM@PoliTO), Politecnico Di Torino, Corso Duca Degli Abruzzi 24, 10129 Turin, Italy

[3] Department of Applied Science and Technology (DISAT), Politecnico Di Torino, Corso Duca Degli Abruzzi 24, 10129 Turin, Italy

of metals, like stainless steel or aluminum alloys, in more demanding application fields, such as sport racing [3], and oil or electrical industries [4, 5]. HPP are thermoplastic polymers with high mechanical performance, thermal stability, and chemical resistance [6]. HPP include both amorphous polymers, such as polyethylenimine (PEI) [7], and semi-crystalline ones, like poly(aryl-ether-ketone) (PAEK) family [8].

Among PAEK polymers, poly(ether-ether-ketone) (PEEK) is probably the most famous and widely used. Due to its unique chemical structure, composed of aromatic rings bonded by ketone and ether groups, it denotes extraordinary thermo-mechanical properties and excellent radiation resistance [9]. For this reason, PEEK may be an ideal material for metal replacement of structural components for aerospace [10], automotive [11], or nuclear power plants [12]. In addition, PEEK is cytocompatible and radio-transparent and can be repeatedly sterilized, so it can be used for various biomedical applications, such as surgical implants and instruments, or dental devices [13, 14].

Various manufacturing techniques are currently employed in the industrial processing of PEEK-based products, including injection molding, extrusion, compression molding, and machining [15–18]. Recently, Additive manufacturing (AM) has also garnered increasing interest in the processing of HPP [19, 20]. In fact, the global market of high-performance polymers for AM was forecast to grow by 24% between 2023 and 2028, with an estimated market of $ 362 million in 5 years [21]. Previous studies demonstrated the possibility of using AM to produce PEEK components without geometry limitations and with relatively low costs [22, 23]. Considering the melt processability of PEEK, both Selective Laser Sintering (SLS) [24] and Fused Filament Fabrication (FFF) [25] were experimented for the realization of 3D printed parts. Although SLS was the first AM technique used for the fabrication of PEEK components, its limited usage compared to FFF is attributed to higher costs and constraints associated with the powder handling.

Fused Filament Fabrication is the most common AM technique to design, develop, and realize thermoplastic polymer parts. In this process, a polymer filament is continuously melted and extruded through a nozzle onto a heated platform to create, layer-by-layer, the final structure [26]. This 3D printing technique offers low manufacturing costs, high flexibility in structural design, prototyping, supervision-free operation, and wide range of available materials [27, 28]. However, the manufacturability of PEEK via FFF meets significant challenges, mostly due to its high melting temperature and its semi-crystalline nature. This last aspect makes PEEK highly subjected to shrinkages during the processing, leading to the formation of defects, geometrical variations or even job failures [29]. Residual stresses can be accumulated during the FFF process, leading to warping and interlayer delamination [30, 31]. All these drawbacks limited the choice of FFF for PEEK in all the applications where quality assurance and reproducibility play a crucial role.

In recent years, several researchers examined the effect of process printing parameters on the final performance of 3D printed PEEK, in terms of print orientation, nozzle temperature, speed, chamber, and platform temperatures [32, 33]. In addition, other authors focused their research on investigating crystallization behavior [34]. The degree of crystallinity and crystal orientation are important parameters to investigate the microstructure and play an important role in the mechanical properties of PEEK component [35, 36]. Notably, for semi-crystalline polymers like PEEK, the degree of crystallinity and crystal orientation can be controlled by heat treatments. Therefore, it was essential for PEEK to investigate the possibility of increasing the crystallinity of 3D printed parts through post-printing heat treatment. In this scenario, annealing represents a valid post-printing heat treatment to enhance the physical and mechanical properties, improve the dimensional stability, and remove any residual stress [37, 38]. However, the published research on the effects of annealing for 3D printing PEEK remains limited. Moreover, the previous works have predominantly focused on conventional heat treatments, involving extended hours in an oven. Yet, a noticeable gap persists in comprehensive investigations into alternative scenarios, offering the potential for shorter and environmentally sustainable manufacturing processes.

Therefore, in this study, a novel approach precisely aimed at exploring these uncharted possibilities was proposed. The primary objective was to evaluate the effect of different annealing processes on the final mechanical properties of PEEK samples obtained by FFF, while also evaluating the crystallization behavior and its influence on the thermal properties. A direct annealing (DA) process, performed simultaneously with the 3D printing, was performed and compared with a traditional post-printing oven annealing (PA). In addition, to assess the overall sustainability of the two different approaches, the energy consumption of the two annealing processes was also evaluated to determine the different cost-effectiveness of the annealing treatments employed.

To the best of the authors' knowledge, studies aimed at improving the crystallization of PEEK components during the FFF process remain extremely limited. This work reports a novel annealing methodology that has the potential to enhance the effectiveness of metal replacement. It is reasonable to think that the innovativeness of this proposed approach could yield positive and substantial impacts across diverse industrial sectors, leading to time and energy savings. Thereby, the sustainability of the HPP manufacturing process via AM can be increased.

2 Materials and methods

2.1 Materials

The poly(ether-ether-ketone) (PEEK) filament was supplied by 3DXTech (3DXTech, Michigan, USA), with commercial name of ThermaX™ and a constant diameter of 1.75 ± 0.05 mm. Before 3D printing, the PEEK spool was oven dried at 120 °C for 4 h to remove any residual moisture.

2.2 3D printing process

A CreatBot PEEK-300 3D printer (CreatBot, Zhengzhou, China) was used in this study to fabricate all kinds of specimens. According to the manufacturer's datasheet, the 3D printer has a maximum building volume of $300 \times 300 \times 400$ mm^3, it is equipped with a dual extruder, which can reach 500 °C, and a nozzle with 0.4 mm diameter was installed. This 3D printer is suitable for processing HPP because it has control over the maximum platform temperature up to 200 °C and over the building chamber up to 140 °C. In addition, the peculiarity that characterizes the machine is the direct annealing (DA) system, which is a patented technology of CreatBot. A heat collector forces a hot air flow on the 3D printed component to perform an annealing treatment simultaneously with the printing polymer deposition.

Two kinds of samples were 3D printed for tensile and compression testing, respectively. The first specimens were realized according to ISO 527 standard, with the shape of type 1BA. The second specimens, according to ISO 604 standard, were realized as cylinders with a diameter of 10 mm, built on the platform plate (XY), and a height of 10 mm (Z-axis). All PEEK samples were designed on SolidWorks CAD software (Dassault Systèmes, Vélizy-Villacoublay, France). Then, the Simplify3D software (Simplify3D, Ohio, USA) was chosen to perform the slicing of all STL (Solid To Layer) models and create the G-code printing files. For all printing jobs, the chosen parameters are listed in Table 1, and the Nano Polymer Adhesive glue (Vision Miner, Oregon, USA) was used on the platform to improve the adherence of the initial printing layers. For both tensile and compressive characterization, four infill percentages were evaluated, namely, 30%, 50%, 70%, and 100%.

Table 1 Process parameters used for the 3D printing of all PEEK specimens

Parameter	Value
Nozzle temperature (°C)	420
Bed temperature (°C)	140
Chamber temperature (°C)	140
Printing speed (mm/s)	25
Layer height (mm)	0.2
Infill pattern	Rectilinear
Infill angle (°)	±45

2.3 Annealing treatment

Two different kinds of heating treatments were performed on the tensile specimens with a 30% infill to compare the mechanical and thermal properties of the 3D printed samples. This specific infill percentage was selected as it represents the worst-case condition for evaluating mechanical properties. In the first case, a hot airflow at 320 °C was directed onto the 3D printed sample simultaneously with the FFF process. Although this heating treatment does not strictly adhere to the conventional definition of annealing process, this was the term employed, aligning with the nomenclature established by the machine producer. Therefore, these samples were coded as "DA," standing for direct annealing. Figure 1 illustrates the Creatbot's patented direct annealing system (DAS), consisting of two fans and two C-shaped additional heaters (Fig. 1a), strategically

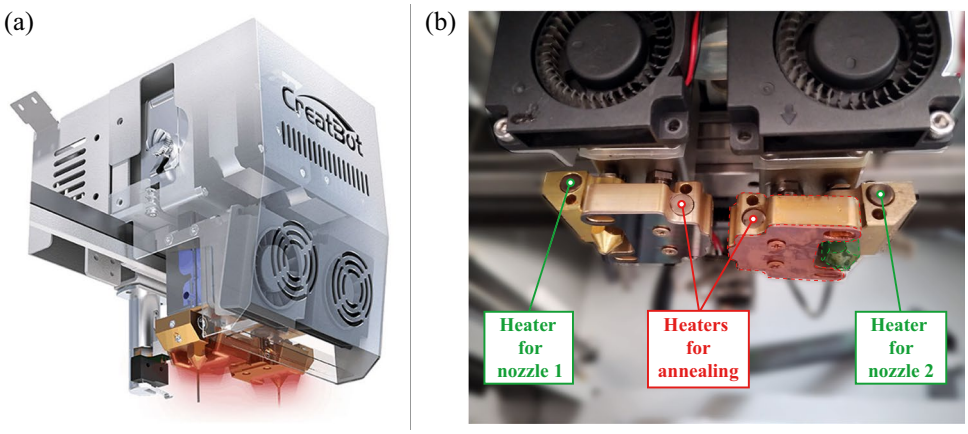

Fig. 1 Direct annealing system patented by Creatbot and reproduced from [39] (**a**). Photo of the printing head with two fans, resistive heating elements for the DA system and extruders (**b**). The bottom surface of the right DAS block is highlighted in red and the right nozzle in green

positioned between the extruders to surround the two nozzles. The DAS heating brass blocks are shown in the photo of Fig. 1b, wherein the right block is highlighted in red and the right nozzle in green. For the DA process, the temperature of each heater can be set separately, and the fan promotes hot airflow in the direction of the build plate. The integrated thermocouple control system enables the activation of the DA system with precise temperature adjustment up to 400 °C. Therefore, when the DAS block is active, additional heat is transferred by irradiation and convection to the area of deposited material that is covered by the motion along the printing path of the specific nozzle. Thus, direct annealing is a local thermal treatment that highly depends on the printing path and geometry of the part because of the fixed relative position between the C-shaped blocks and the nozzles.

The second type of heat treatment involved traditional annealing in the oven, after the 3D printing. Specifically, the samples were brought from room temperature to 200 °C and left at this temperature for 2 h. Then, the temperature was lowered to 140 °C at a 10 °C/hour rate, and finally the oven was turned off to go back to room temperature. These samples were coded as "PA" for post annealing. To better investigate the effect of the annealing processes, the final properties were also compared with unannealed samples, referred to as "NA" for not annealed, and with the as-received PEEK filament, referred to as "AR."

2.4 Characterization techniques

2.4.1 Differential scanning calorimetry (DSC)

Differential scanning calorimetry (DSC) analyses were carried out using a DSC 214 Polyma Equipment (Netzsch Group, Selb, Germany). Two heating and cooling scans were performed under a nitrogen atmosphere (40 mL/min) from 20 to 400 °C with a heating/cooling rate of 10 °C/min. DSC analysis was performed to determine the glass transition temperature (T_g), the melting temperature (T_m), the crystallization temperature (T_c), the cold crystallization temperature (T_{cc}), their associated enthalpies of fusion (ΔH_m), crystallization (ΔH_c), and cold crystallization (ΔH_{cc}). The degree of crystallization (X_c) for all PEEK samples was estimated using the following equation:

$$X_c = \frac{\Delta H_m - \Delta H_{cc}}{\Delta H_m^0} \times 100 \quad (1)$$

where ΔH_m is the experimental enthalpy of melting, calculated by the integration of the melting endothermic peak, ΔH_{cc} is the enthalpy of cold crystallization, and ΔH_m^0 is the theoretical melting enthalpy of a purely crystalline PEEK, which was assumed to be equal to 130 J/g [40].

2.4.2 Thermogravimetric analysis (TGA)

Thermogravimetric (TG) analysis was carried out to investigate the thermal stability of the 3D printed PEEK samples using a Mettler-Toledo TGA 851e instrument (Mettler Toledo, Columbus, Ohio, USA). The samples were heated from 25 to 1000 °C at a heating rate of 10 °C/min under an airflow of 50 mL/min. All the TG curves were normalized to the unit weight of the PEEK samples, and the derivative thermogravimetric (DTG) curves were calculated on their relative thermograms.

2.4.3 Tensile tests

The uniaxial tensile tests were performed, according to ISO 527 standard, on all 3D printed PEEK specimens. The Aura 5 T machine (Easydur, Arcisate, Italy), equipped with a 50 kN load cell, was used with a crosshead speed of 1 mm/min and a pre-load of 150 N. Five specimens were tested for each condition.

2.4.4 Compression tests

The uniaxial compression tests were performed, according to ISO 604 standard, on 3D printed PEEK specimens, which were subjected to PA treatment. The Aura 5 T machine (Easydur, Arcisate, Italy), equipped with a 50 kN load cell, was used with a crosshead speed of 5 mm/min. Five specimens were tested for each infill percentage.

2.4.5 Energy consumption

All PEEK samples were weighed with a Gibertini balance (Gibertini, Novate Milanese, Italy), and the effective dimensions were measured with a micrometer. In addition, the power consumption for 3D printing PEEK samples was measured with a Meterk M34EU power meter plug.

3 Results and discussion

3.1 Effect of annealing and heated chamber on sample appearance

A preliminary visual analysis of the samples was carried out to qualitatively appreciate the effect of the different thermal treatments performed on the 3D printed PEEK samples, i.e., no annealing (NA), direct annealing (DA), and post annealing (PA). As a representative example of all the manufactured samples, Fig. 2 illustrates the appearance of three tensile specimens, each corresponding to a different thermal approach. The NA tensile sample, highlighted in red, exhibited initial layers of a darker color

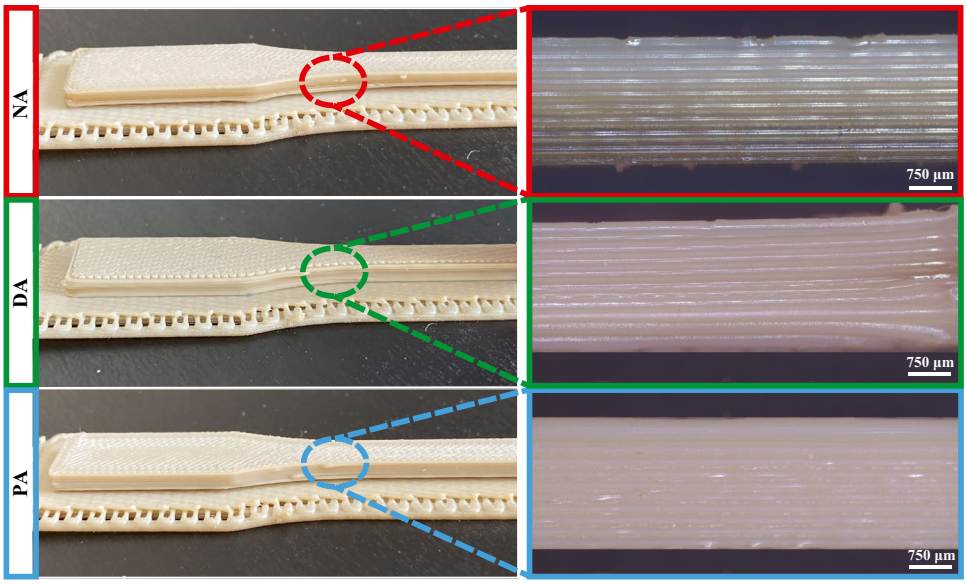

Fig. 2 Macroscopic effect of different annealing treatments

compared to the final ones. In contrast, the DA specimen displayed a more uniformly colored surface, except for certain details highlighted in the green magnified area. However, it is evident that the PA sample possesses the most consistently uniform coloration along the entire build direction.

As already suggested in the previous literature, this diversity of colors can be attributed to a different degree of crystallinity. In particular, a darker coloration can be indicative of an amorphous zone, while the beige zone is typical of areas with a higher degree of crystallinity [33]. The difference in appearance, and thus the degree of crystallinity, can be attributed to the different cooling rates, which was sufficiently controlled in both annealing cases to achieve higher polymer crystallinity, compared to the NA condition. However, there are limited brownish regions in the DA samples suggesting that the annealing did not occur uniformly everywhere, and hence a slightly lower degree of crystallinity can be expected for these samples, compared to the PA condition. Overall, it can be assumed that both annealing processes positively affected the uniformity of coloration and thermal properties of the samples, thus suggesting to be an important step in PEEK 3D printing.

Another aspect that was initially examined was the importance of the heated chamber for 3D printing of PEEK by FFF. In fact, in our previous study, it was found that the compression properties of small PEEK cylinders were not significantly affected by the chamber temperature [41]. However, here, the critical role of the heated chamber in avoiding warpage, geometric distortion, and detachment of the specimens from the platform, which could lead to printing abortion, was immediately appreciated. As a matter of fact, 3D printing of larger geometries, such as that of tensile samples compared to compression cylinders, increases the deposition time between successive layers [42]. This is the reason why the first printing trial conducted without a heated chamber caused the samples to warp and detach from the platform, as shown in Fig. 3a. Secondly, it was recognized the significant effect of the raft, which could prevent the deformation of the first layer, as visible in Fig. 3b, c, where sample pictures were taken from the bottom layer, showing a widening of the first layer compared to the nominal 5-mm width. Therefore,

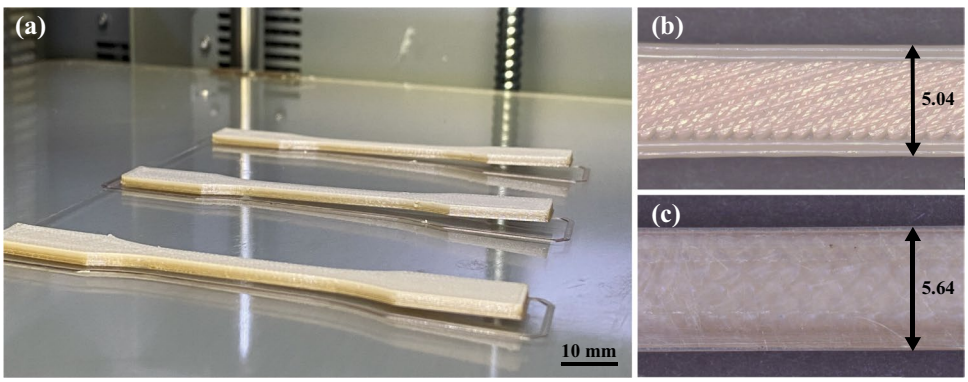

Fig. 3 Photograph of the detachment from the platform of the tensile specimens 3D printed without a heated chamber (**a**). Bottom layer of a tensile specimen 3D printed with raft (**b**) and without raft (**c**). All dimensions in mm

all experimental samples, whose results will be presented from here on, were 3D printed in a hot chamber (140 °C) with 4 layers of raft.

3.2 Thermal characterization

In order to gain a more thorough understanding of the impact of various annealing processes on the crystallization behavior and thermal properties of 3D printed PEEK samples, we conducted DSC and TGA analyses. DSC analysis was performed to determine the thermal transitions: the glass transition temperature (T_g), the melting temperature (T_m), the crystallization temperature (T_c), the cold crystallization temperature (T_{cc}), and their relative enthalpies. All the data obtained by DSC are summarized in Table 2.

Figure 4 shows the DSC curves of the PEEK samples as received (AR), 3D printed by FFF with annealing (PA and DA), and without annealing (NA), relative to the first and second heating/cooling cycle, as reported in Fig. 4a, b, respectively.

Following the first heating scan in Fig. 4a, a glass transition is evident between 140 and 160 °C, followed by a marked cold crystallization exothermic peak approximately at 176 °C, only for the NA sample. This can be explained considering that the cooling rate of the unannealed 3D printed sample can reach tens of degrees per minute during FFF, and therefore, the polymer does not have sufficient time to properly crystallize [43]. This explanation was confirmed by the absence of cold crystallization peaks for the annealed samples, where the heat treatments allowed the polymer chains to reorganize and form a semi-crystalline structure, which did not lead to further crystallization during the first heating. In addition, by determining the experimental enthalpy of fusion (ΔH_m) and cold crystallization (ΔH_{cc}), it was possible to calculate the degree of crystallinity (X_c) of the PEEK samples and then evaluate the real effect of the annealing on the polymer crystallinity. The X_c of PEEK samples was calculated both on the first and the second heating cycles, following Eq. 1. Considering the first heating cycle, the crystallinity percentage was 28.5% for both AR and DA samples. Thus, the DA printing process did not thermally alter the crystallinity of the material. On the other hand, an X_c value of 16.6% was obtained for the NA sample, due to the cold crystallization phenomenon occurring during the first heating. This result implies that the state of lower crystallinity must necessarily be reached during 3D printing without annealing, and it confirmed what was previously found from the visual analysis of the printed specimens. Considering the second heating scan, where the thermal history of the samples was erased by the first heating and cooling cycles, the X_c values obtained were 24.7% and 25.9% for the unannealed samples, and 32.1% and 34.9% for the PA and DA ones, respectively. The higher value of the degree of crystallinity after annealing can be due to greater molecular mobility occurring during the heating treatments, which enabled the polymer chains to reorient and form a

Table 2 Thermal properties of 3D printed PEEK samples, evaluated by DSC analysis in nitrogen

Sample	1st heating					Cooling		2nd heating			
	T_{cc} (°C)	ΔH_{cc} (J/g)	T_m (°C)	ΔH_m (J/g)	X_c (%)	T_c (°C)	ΔH_c (J/g)	T_g (°C)	T_m (°C)	ΔH_m (J/g)	X_c (%)
PEEK AR	/	/	340	37.1	28.5	296	47.4	140	340	47.3	24.7
PEEK NA	176	17.9	340	39.4	16.6	294	50.8	145	339	41.2	25.9
PEEK PA	/	/	338	38.0	29.2	295	53.6	154	340	41.7	32.1
PEEK DA	/	/	338	37.1	28.5	295	48.5	153	340	45.3	34.9

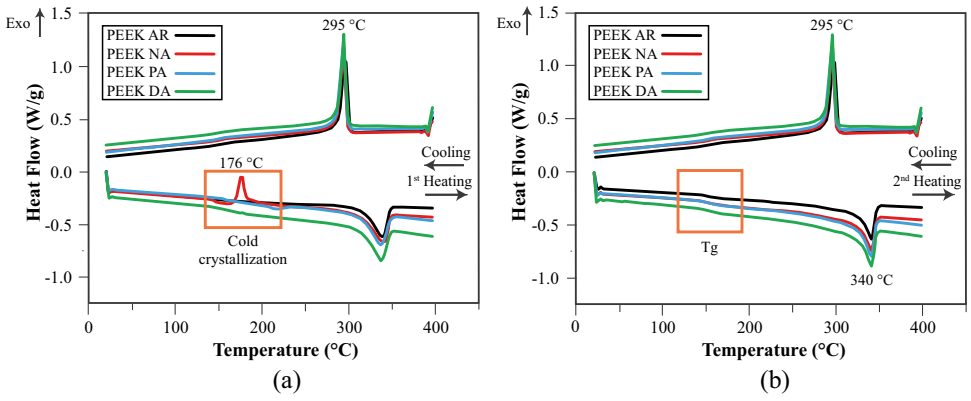

Fig. 4 DSC curves of PEEK samples related to the cooling cycle plus the first (**a**) and second (**b**) heating cycle

more ordered crystalline structure [44]. In fact, PEEK as a semi-crystalline polymer when exposed to high temperatures can show changes in phase composition and thus in the molecular mobility of the different crystalline domains.

Analyzing the cooling scans, all PEEK samples exhibited a single crystallization peak at approximately 295 °C. Besides, as shown in Fig. 4, similar melting state transitions were observed for all samples, which had a single broad endothermic peak at about 340 °C, independently from sample type and heating cycle.

Moreover, the second heating scans clearly revealed the T_g values, located at 140 °C for the PEEK AR, and 145 °C for the NA samples. The values of the glass transition temperature shifted towards higher temperatures, approximately at 154 °C for both DA and PA samples, as shown in the curves of Fig. 4b. It is noteworthy that the T_g values of the annealed PEEK samples are significantly higher than those of the as-received or not annealed samples. This trend was already observed in the previous literature [45]. The increase of the glass transition temperature can be explained considering that the annealing of semi-crystalline polymers, like PEEK, not only changes the crystalline structure and the degree of crystallinity but also affects the amorphous phase mobility. Annealing treatment reduces the chain mobility of the rigid fraction of the amorphous phase, leading to an increase of the T_g values [44].

The thermal stability of the PEEK samples was evaluated through TG analysis in air. The thermogravimetric curves and their relative first derivatives for PEEK samples are shown in Fig. 5a, b, respectively.

From these curves, it can be clearly observed that the thermal degradation of PEEK in air involves two main steps. The first begins approximately at 585 °C, evaluated as a relative maximum of the DTG curves, and corresponds to the chain scission of the ether and ketone bonds [46], whereas, for temperatures higher than 660 °C, the second decomposition step occurs, due to the cracking of the aromatic crosslinked residue produced during the first stage of degradation [46]. These findings are consistent with the previous literature and suggest that a thermodynamically stable char structure is formed during the first step of PEEK degradation, which is then decomposed in a second step at high temperatures (Fig. 5b) [47]. Consequently, when the material is subjected to high temperatures, the PEEK 3D printed samples form a char that can act as a thermal and physical barrier, limiting heat conduction to the bulk of the polymer material and retarding decomposition. Similar trends have already been found in previous studies, including other polymer matrices [48].

For all samples, thermal stability was assessed by determining the initial degradation, evaluated as the temperature corresponding to 5% weight loss (T_5), and the degradation temperature at which 50% weight loss is achieved (T_{50}), as reported in Table 3.

All T_5 values are quite similar, regardless of whether the samples were PEEK NA (567 °C), PEEK PA (570 °C), or PEEK DA (572 °C). The same behavior was observed for the T_{50} values, which were approximately 645 °C for all samples. However, the annealing process positively affected the maximum degradation temperatures of the 3D printed component. In fact, the second DTG degradation peak ($T_{\text{deg peak2}}$) for PEEK DA was 29 °C higher than that of PEEK NA (Fig. 5b). It is also noteworthy that there is a significant influence of thermal stability even among 3D printed PEEK samples considering the two different annealing treatments. In fact, if the post annealing leads to a very poor increase in thermal stability, i.e., from 665 to 667 °C, the direct

Table 3 Thermal properties of 3D printed PEEK samples evaluated by TG analysis performed in air

Sample	T_5 (°C)	T_{50} (°C)	$T_{\text{deg peak1}}$ (°C)	$T_{\text{deg peak2}}$ (°C)
PEEK AR	567	645	585	665
PEEK NA	566	645	585	654
PEEK PA	570	645	585	667
PEEK DA	572	645	585	683

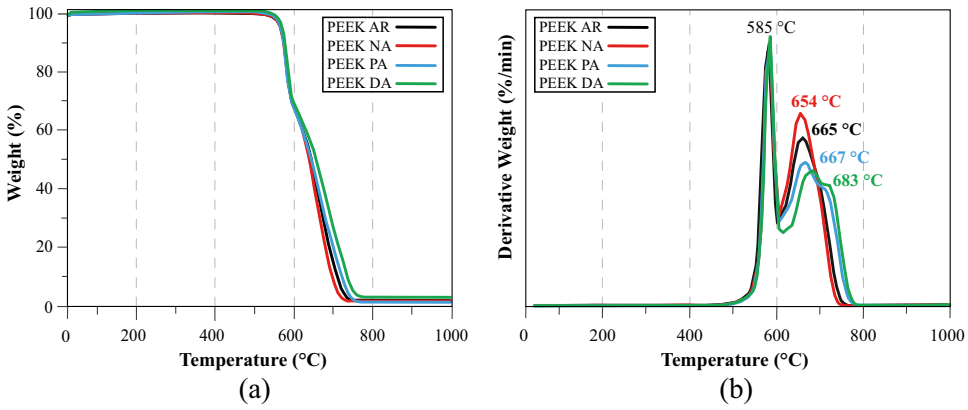

Fig. 5 Thermogravimetric curves of PEEK samples (**a**) and their DTG curves (**b**)

annealing process seems to promote a significant increase in degradation temperature, with a $T_{\text{deg peak2}}$ at 683 °C.

3.3 Mechanical characterization

Tensile and compression tests were performed to evaluate the influence of the two annealing treatments on the mechanical properties of 3D printed PEEK samples. Specifically, the tensile and compression measurements were performed on specimens with 30% infill that underwent both PA and DA treatments. This investigation aimed to examine the variations in the mechanical behavior of PEEK specimens, particularly under the worst-case infill conditions. Additionally, this approach was designed to minimize the use of PEEK, given its high material cost, demonstrating a strategic balance between thorough analysis and resource efficiency. In addition, NA tensile samples were tested for comparison, and the results in terms of Young's modulus (E) and ultimate tensile strength (UTS) are illustrated in Fig. 6. It is evident that both annealing treatments enhanced the tensile properties and uniformity of the printed parts, thereby improving reproducibility and leading to a lower standard deviation. The superior mechanical performance of PA samples is consistent with the previous literature, confirming that an annealing process can significantly improve stiffness. These results are also in line with the calculated degree of crystallinity [49, 50]. Considering the DA samples, it can be assumed that in addition to the heated platform and building chamber, a local heat flow could help improving the entanglement between polymer chains, resulting in stronger adhesion and superior mechanical properties [51, 52]. Therefore, the improvement in the mechanical performance of the DA samples might be due to the heat collector on the nozzle head, which provided uniform temperature around the nozzle and slowed the cooling rate of the extruded polymer during printing. Moreover, the heat collector might soften the previous layer, also improving the interlayer adhesion. In fact, the adhesion process between two successive layers could be schematized in two steps, the first one is the initial contact and neck growth between them; the second one is molecular diffusion and randomization at the interface. This last step depends on the entanglement process between the polymer chains of the two consecutive layers. This process is known to be enhanced by reducing the temperature gradient between the extruded filament and the preceding one [51–53]. However, the local heat flow supplied during printing proves inadequate for relieving all internal defects and residual stress, potentially resulting in lower mechanical performance of PEEK parts [54]. Notably, Young's modulus of the DA samples is inferior compared to that of PA sample, indicating lower stiffness. Therefore, to evaluate the effect of the infill percentage on mechanical properties, all specimens underwent PA treatments.

Figure 7 illustrates the influence of infill percentage over E and UTS, as well as over their specific values. The specific Young's modulus (E*) and the specific ultimate tensile strength (UTS*) were calculated by dividing E and UTS, respectively, by the mass density of each specimen. Young's modulus and UTS exhibited an average increase of about 26% and 39%, respectively, as the infill percentage raises from 30 to 100%. It is clear that the infill percentage directly affected the mechanical properties of 3D printed samples due to the amount of deposited material and the variation in sample cross-section [55]. In Fig. 7, the orange trend lines illustrate the values of the specific tensile properties for both E* and UTS*. As the infill percentage increases, there is a linear improvement in these properties up to 70% infill. Above this percentage, both E* and UTS* decrease, suggesting that 70% infill could be an interesting value in terms of material optimization for tensile load applications. These findings are consistent with previous studies. For example, Rinaldi et al. observed that the material deposited is poor below 50% infill, so the outer perimeter mainly bears the tensile load [56].

The compressive behavior of 3D printed samples was characterized by compression tests, and the key results are shown in Fig. 8 for the lowest and highest infill percentages. In addition, Fig. 9 summarizes the compressive strengths and modulus, as well as their specific values, for all infill percentages. In Fig. 8, all compressive stress and strain curves

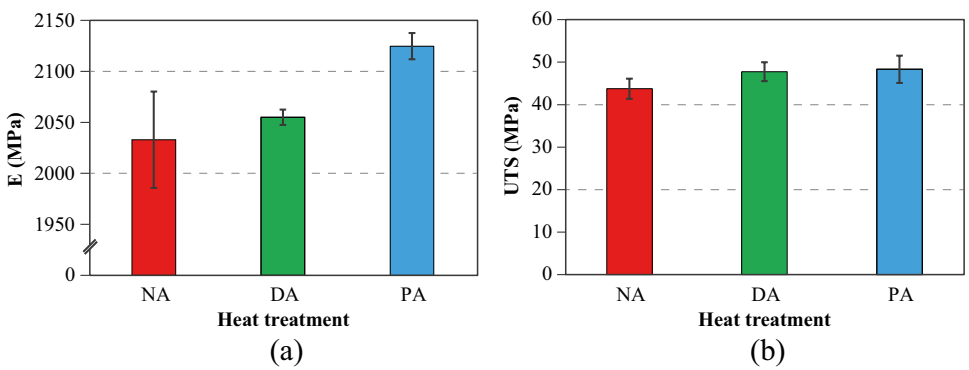

Fig. 6 Comparison of different heating treatments on tensile properties: Young's modulus (**a**) and ultimate tensile strength (**b**)

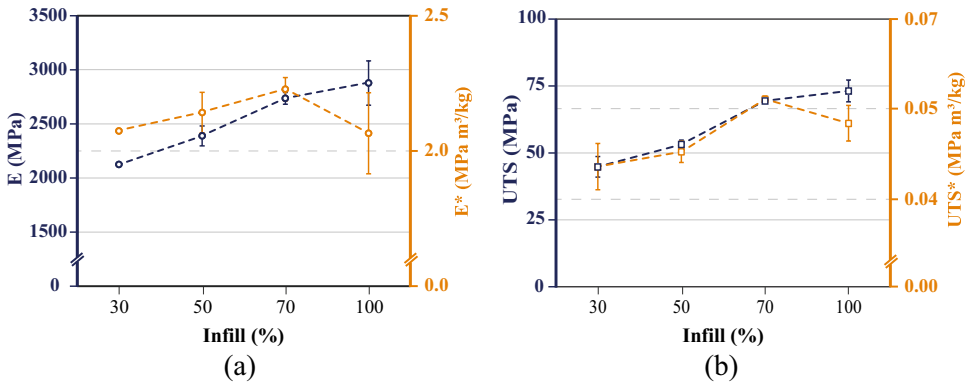

Fig. 7 Comparison of different infill percentages for tensile properties: Young's modulus (**a**) and ultimate tensile strength (**b**)

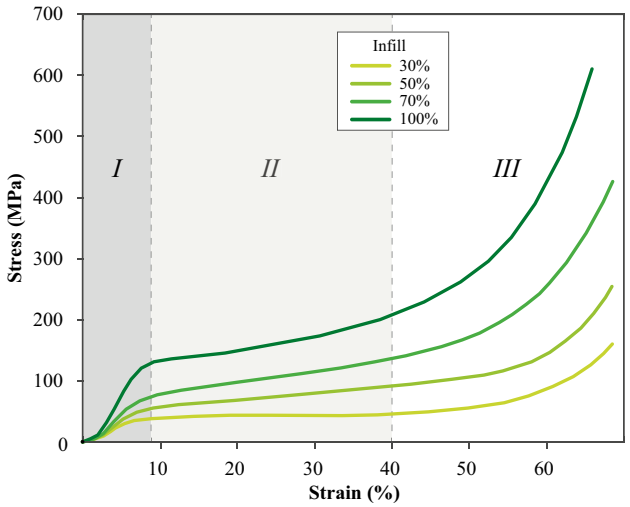

Fig. 8 Stress–strain curves for compression testing with four different infill percentages: 30%, 50%, 70%, and 100%. Three stages: (I) linear elasticity, (II) plateau, and (III) densification

revealed three distinct regions: a zone of linear elasticity (I), a plateau (II), and a densification region (III), in line with typical compressive curves [57]. After the first elastic deformation (I) and during the second stage (II), the sample's internal structure deformed with almost no increase in density. Figure 8 shows that the plateau length decreases proportionally with the increase in infill percentage, due to a greater volume of extruded material and, consequently, a reduced possibility of rearrangement of the internal structure. In the third stage (III), stress increased with a less significant increase in deformation, as the samples began to compress as bulk material, resulting in a rapid increase in the sample resistance. These experimental results are consistent with previous research in the literature [58–61], and the compressive performance increased for increasing infill percentages, as expected. The compressive strength, evaluated at strain of 20%, increased from 46.7 ± 1.6 MPa for 30% infill to 147.2 ± 1.9 MPa for 100% infill. A similar increase of approximately 35% was also observed for the compressive modulus, varying from 741.4 ± 12.8 MPa for 30% infill to 2122.0 ± 161.4 MPa for 100% infill.

However, comparing the infill percentages in terms of specific compressive properties, the highest value for the specific compressive modulus was again identified in the 70% infill density samples, as shown by the orange lines in Fig. 9a. Therefore, choosing a 70% infill could be advantageous for applications necessitating mass optimization to achieve a lightweight design. Conversely, when assessing the specific compressive strength, evaluated at strain of 20%, it is notable that the samples with 100% infill demonstrated superior properties compared to all other samples.

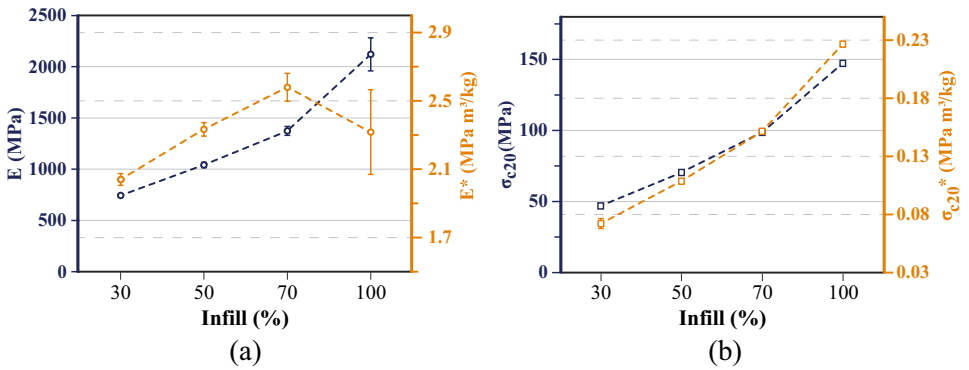

Fig. 9 Comparison of different infill percentages for compression properties: compressive modulus (**a**) and compressive strength evaluated at 20% strain (**b**)

3.4 Energy consumption

For a preliminary assessment of the sustainability of the different processes examined, the production time and the energy consumption were measured and expressed as a function of the heat treatment and infill percentage of the various samples. It was then noteworthy to relate these results to the previously presented mechanical properties.

Table 4 presents the effect of the different annealing treatments on production time and energy consumption. It is evident that with the DA approach, a great amount of time can be saved in comparison to the PA treatment, which involves keeping the samples in the oven for more than 8 h. In addition, the findings indicated that the PA treatment is the process with the greatest impact on the overall energy consumption. However, it is very important to point out that, in the data shown in Table 4, all the energy (2.7 kWh) required for annealing in the oven was attributed to a single specimen. Certainly, this value can be drastically reduced by saturation of the oven volume. However, the most interesting consideration that can be drawn from these results is that the energy consumption increment due to the DA treatment is almost negligible. Therefore, it can be concluded that DA treatment, for a slight decrease in the mechanical performance if compared with the PA treatment, can considerably reduce the production cycle time and energy requirement.

Furthermore, Table 5 and 6 show the effect of the different infill percentages on printing time and energy consumption to produce tensile and compression specimens, respectively. For both kinds of samples, the same trend was observed.

In fact, as the infill percentage increases, there is a slight increase in printing time due to the higher amount of deposited material, which was also evidenced by the rise in sample weight. In addition, the increased printing time resulted in a marginally higher energy absorption.

However, it is very interesting to note a decreasing trend in energy consumption when normalized to the mass of the samples. In fact, the specific energy consumption, defined as the ratio of energy consumption to produce a sample to its mass, drops as the infill percentage increases. This observation is particularly significant given the mechanical test results, which demonstrated optimal performance at higher infill percentages, approximately 70% for both tensile and compression tests. There is little previous research focusing on energy consumption in 3D printing of HPP using FFF. Besides, in the few existing studies, it is often challenging to align the material [62] or influencing parameters considered [63, 64] with those presented here. However, the results of this research are consistent with those reported by Hassan et al., who investigated the effect of infill percentages and patterns on the energy consumption of FFF for carbon-fiber-reinforced PEEK [65].

To briefly summarize the analyses conducted so far, Fig. 10 illustrates the sequential steps undertaken in the preceding sections, providing a visual representation of the systematic approach adopted and presenting the corresponding results in each step. The preliminary results of this study are promising and deserve further investigation to reach a more comprehensive understanding of the heating treatment and its impact on 3D printed samples. Conducting a thermofluidic dynamics analysis of the heating system could provide insights into the consistency of the annealing treatment. Moreover, a more in-depth characterization of the effects of DA on thermodynamo mechanical properties of the samples would be valuable. This analysis could simulate more challenging environments for the samples thus shedding light on their possible application in fields such as chemical, aerospace, or racing industries.

Table 4 Effect of different annealing processes on production time and energy consumption for 3D printing of PEEK samples

Parameter	NA	PA	DA
Production time (min)	22	502	22
Energy consumption (kWh)	0.49	3.18*	0.52

*All the energy required for annealing in oven was attributed to a single specimen

Table 5 Effect of infill percentage on printing time and energy consumption for the 3D printing of PEEK tensile samples

Parameter	Infill percentage			
	30%	50%	70%	100%
Printing time (min)	22	23	24	25
Energy consumption (kWh)	0.50	0.51	0.53	0.55
Sample mass (g)	3.89	3.99	4.25	4.53
Specific energy consumption (kWh/g)	0.129	0.127	0.125	0.121

Table 6 Effect of infill percentage on printing time and energy consumption for the 3D printing of PEEK compression samples

Parameter	Infill percentage			
	30%	50%	70%	100%
Printing time (min)	7	8	9	10
Energy consumption (kWh)	0.19	0.20	0.21	0.23
Sample mass (g)	0.95	1.08	1.21	1.39
Specific energy consumption (kWh/g)	0.200	0.185	0.174	0.165

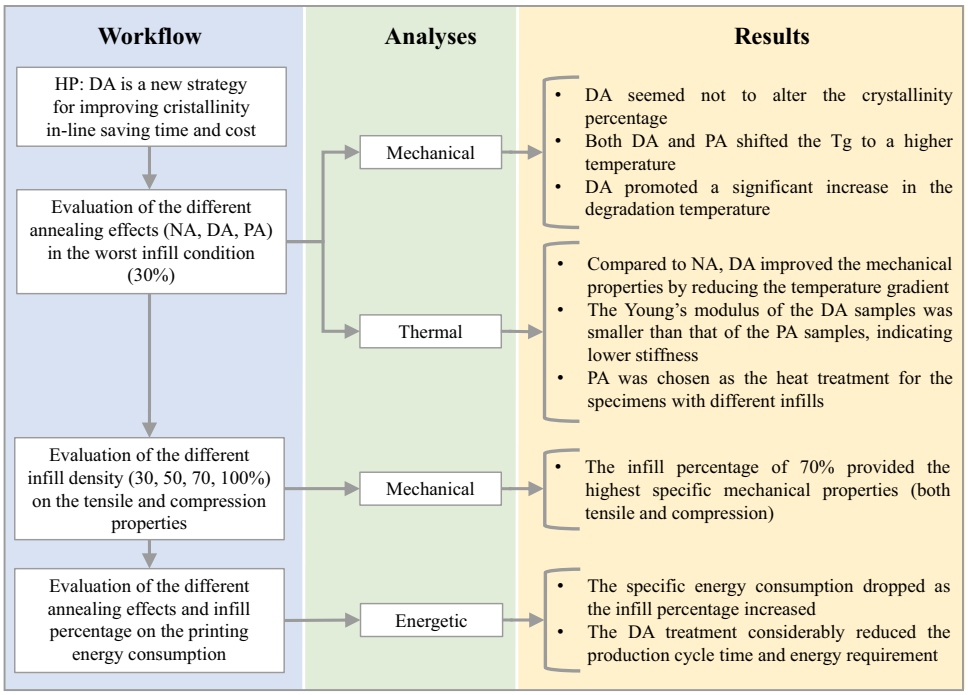

Fig. 10 Scheme of the logical workflow of research, highlighting the main analyses and related results

4 Conclusions

This research aimed to investigate the effect of two different annealing approaches and the influence of the infill percentage on the thermal properties, mechanical performance, and energy consumption required for 3D printing of PEEK components using Fused Filament Fabrication. The research outcomes suggest that both direct annealing (DA) and post annealing (PA) positively influenced the thermal properties of PEEK, leading to a higher degree of crystallinity and a delayed onset temperature of degradation. The final component treated with DA exhibited higher thermal stability, as evidenced by a higher second degradation peak, in comparison to the PA sample.

The effect of the different annealing processes on tensile properties was investigated and indicated that the highest stiffness was achieved by PA. However, the DA specimens also demonstrated an enhancement in Young's modulus and UTS compared with unannealed (NA) samples. In addition, the influence of the infill percentage on mechanical properties showed a similar trend for both tensile and compressive test results. While absolute properties increased with higher infill percentages, the peak values in terms of specific properties were obtained at approximately 70% infill, resulting in time and material savings compared to fully dense samples.

Relating the energy required to print the various samples with the final mechanical performance from compressive and tensile tests provided valuable insights into the eco-efficiency of FFF processing of PEEK. It could be suggested that 3D printing a component with DA results in substantial energy and time savings, making it advantageous even if a modest oversizing may be required to compensate for the lower mechanical properties of a PA part.

In conclusion, this research highlighted the advantages of the DA approach, demonstrating significant improvements in energy consumption, production time, and thermal stability when compared to traditional PA method. However, it is crucial to acknowledge that the mechanical performance achieved through this approach was still lower compared to that obtained through post annealing. To address this limitation, further investigation into the DA process is worthy, with a potential focus on optimization strategies, including real-time control of heat flow. By adopting this strategy, the full potential of the direct annealing approach could be developed, also aligning the mechanical performance with that provided by conventional heat treatment in oven. Nevertheless, the findings of this study are promising and pave the way for further research towards the processability of high-performance polymers through AM, making metal replacement more industrially accessible.

Funding Open access funding provided by Politecnico di Torino within the CRUI-CARE Agreement. This study was carried out within the Ministerial Decree no. 1062/2021 and received funding from the FSE REACT-EU-PON Ricerca e Innovazione 2014–2020. This manuscript reflects only the authors' views and opinions, neither the European Union nor the European Commission can be considered responsible for them.

Declarations

Conflict of interest The authors declare no competing interests.

Open Access This article is licensed under a Creative Commons Attribution 4.0 International License, which permits use, sharing, adaptation, distribution and reproduction in any medium or format, as long as you give appropriate credit to the original author(s) and the source, provide a link to the Creative Commons licence, and indicate if changes were made. The images or other third party material in this article are included in the article's Creative Commons licence, unless indicated otherwise in a credit line to the material. If material is not included in the article's Creative Commons licence and your intended use is not permitted by statutory regulation or exceeds the permitted use, you will need to obtain permission directly from the copyright holder. To view a copy of this licence, visit http://creativecommons.org/licenses/by/4.0/.

References

1. Lu K (1979) (2010) The future of metals. Science 328:319–320. https://doi.org/10.1126/science.1185866
2. Bertagna S, Braidotti L, Laurini E et al (2022) Thermoplastic materials for the metal replacement of non-structural components in marine engines. Appl Sci 12:8766. https://doi.org/10.3390/app12178766
3. Tong Y (2019) Application of polymer materials with high mechanical properties in competitive sports. IOP Conf Ser Mater Sci Eng 612:32094. https://doi.org/10.1088/1757-899X/612/3/032094
4. de Leon ACC, da Silva ÍGM, Pangilinan KD et al (2021) High performance polymers for oil and gas applications. React Funct Polym 162:104878. https://doi.org/10.1016/j.reactfunctpolym.2021.104878
5. He M, Qiu F, Lin Z (2013) Towards high-performance polymer-based thermoelectric materials. Energy Environ Sci 6:1352–1361. https://doi.org/10.1039/C3EE24193A
6. Avci H, Hassanin A, Hamouda T, Kılıç A (2019) High performance fibers: a review on current state of art and future challenges. Eskişehir Osmangazi Üniversitesi Mühendislik ve Mimarlık Fakültesi Dergisi 27:130–155
7. Chen Z, Lv Z, Sun Y et al (2020) Recent advancements in polyethyleneimine-based materials and their biomedical, biotechnology, and biomaterial applications. J Mater Chem B 8:2951–2973. https://doi.org/10.1039/C9TB02271F
8. Zol SM, Alauddin MS, Said Z et al (2023) Description of poly(aryl-ether-ketone) materials (PAEKs), polyetheretherketone (PEEK) and polyetherketoneketone (PEKK) for application as a dental material: a materials science review. Polymers (Basel) 15:2170. https://doi.org/10.3390/polym15092170
9. Ling X, Jing X, Zhang C, Chen S (2020) Polyether ether ketone (PEEK) properties and its application status. IOP Conf Ser Earth Environ Sci 453:12080. https://doi.org/10.1088/1755-1315/453/1/012080
10. Shekar RI, Kotresh TM, Rao PMD, Kumar K (2009) Properties of high modulus PEEK yarns for aerospace applications. J Appl Polym Sci 112:2497–2510. https://doi.org/10.1002/app.29765
11. Pradeep SA, Iyer RK, Kazan H, Pilla S (2017) 30 - Automotive applications of plastics: past, present, and future. In: Kutz M (ed) Applied Plastics Engineering Handbook, 2nd edn. William Andrew Publishing, Second Edition, pp 651–673
12. Khare N, Limaye PK, Soni NL, Patel RJ (2015) Gamma irradiation effects on thermal, physical and tribological properties of PEEK under water lubricated conditions. Wear 342–343:85–91. https://doi.org/10.1016/j.wear.2015.08.005
13. Senra MR, de Marques M, FV, Monteiro SN, (2023) Poly (ether-ether-ketone) for biomedical applications: from enhancing bioactivity to reinforced-bioactive composites&mdash. An Overview. Polymers (Basel) 15:373. https://doi.org/10.3390/polym15020373
14. Verma S, Sharma N, Kango S, Sharma S (2021) Developments of PEEK (Polyetheretherketone) as a biomedical material: a focused review. Eur Polym J 147:110295. https://doi.org/10.1016/j.eurpolymj.2021.110295
15. Li T, Song Z, Yang X, Du J (2023) Influence of processing parameters on the mechanical properties of peek plates by hot compression molding. Materials 16:36. https://doi.org/10.3390/ma16010036
16. Xu J, Huang X, Davim JP et al (2020) On the machining behavior of carbon fiber reinforced polyimide and PEEK thermoplastic composites. Polym Compos 41:3649–3663. https://doi.org/10.1002/pc.25663
17. Gul S, Arican S, Cansever M et al (2023) Design of highly thermally conductive hexagonal boron nitride-reinforced PEEK composites with tailored heat conduction through-plane and rheological behaviors by a scalable extrusion. ACS Appl Polym Mater 5:329–341. https://doi.org/10.1021/acsapm.2c01534
18. Zhao J, Guo C, Zuo X et al (2022) Effective mechanical properties of injection-molded short fiber reinforced PEEK composites using periodic homogenization. Adv Compos Hybrid Mater 5:2964–2976. https://doi.org/10.1007/s42114-022-00518-y
19. Weyhrich CW, Long TE (2022) Additive manufacturing of high-performance engineering polymers: present and future. Polym Int 71:532–536. https://doi.org/10.1002/pi.6343
20. de Leon AC, Chen Q, Palaganas NB et al (2016) High performance polymer nanocomposites for additive manufacturing applications. React Funct Polym 103:141–155. https://doi.org/10.1016/j.reactfunctpolym.2016.04.010
21. https://www.marketsandmarkets.com/Market-Reports/3d-printing-high-performance-plastic-market-216044197.html. Accessed 19 Oct 2023
22. Dua R, Rashad Z, Spears J et al (2021) Applications of 3D-printed PEEK via fused filament fabrication: a systematic review. Polymers (Basel) 13:4046. https://doi.org/10.3390/polym13224046
23. Francis JN, Banerjee I, Chugh A, Singh J (2022) Additive manufacturing of polyetheretherketone and its composites: a review. Polym Compos 43:5802–5819. https://doi.org/10.1002/pc.26961
24. Hoskins TJ, Dearn KD, Kukureka SN (2018) Mechanical performance of PEEK produced by additive manufacturing. Polym Test 70:511–519. https://doi.org/10.1016/j.polymertesting.2018.08.008
25. Arif MF, Kumar S, Varadarajan KM, Cantwell WJ (2018) Performance of biocompatible PEEK processed by fused deposition additive manufacturing. Mater Des 146:249–259. https://doi.org/10.1016/j.matdes.2018.03.015
26. Gao X, Qi S, Kuang X et al (2021) Fused filament fabrication of polymer materials: a review of interlayer bond. Addit Manuf 37:101658. https://doi.org/10.1016/j.addma.2020.101658
27. Cao D, Bouzolin D, Lu H, Griffith DT (2023) Bending and shear improvements in 3D-printed core sandwich composites through modification of resin uptake in the skin/core interphase region. Compos B Eng 264:110912. https://doi.org/10.1016/j.compositesb.2023.110912
28. Cao D (2023) Investigation into surface-coated continuous flax fiber-reinforced natural sandwich composites via vacuum-assisted material extrusion. Progress in Additive Manufacturing. https://doi.org/10.1007/s40964-023-00508-6
29. Zanjanijam AR, Major I, Lyons JG et al (2020) Fused filament fabrication of PEEK: a review of process-structure-property relationships. Polymers (Basel) 12:1665. https://doi.org/10.3390/polym12081665
30. Yadav A, Rohru P, Babbar A et al (2022) Fused filament fabrication: a state-of-the-art review of the technology, materials,

properties and defects. Int J Interactive Des Manuf (IJIDeM) 17:2867–2889. https://doi.org/10.1007/s12008-022-01026-5
31. Gao R, Xie J, Yang J et al (2021) Research on the fused deposition modeling of polyether ether ketone. Polymers (Basel) 13:2344. https://doi.org/10.3390/polym13142344
32. Jiang C-P, Cheng Y-C, Lin H-W et al (2022) Optimization of FDM 3D printing parameters for high strength PEEK using the Taguchi method and experimental validation. Rapid Prototyp J 28:1260–1271. https://doi.org/10.1108/RPJ-07-2021-0166
33. Challa BT, Gummadi SK, Elhattab K et al (2022) In-house processing of 3D printable polyetheretherketone (PEEK) filaments and the effect of fused deposition modeling parameters on 3D-printed PEEK structures. Int J Adv Manuf Technol 121:1675–1688. https://doi.org/10.1007/s00170-022-09360-4
34. Doumeng M, Makhlouf L, Berthet F et al (2021) A comparative study of the crystallinity of polyetheretherketone by using density, DSC, XRD, and Raman spectroscopy techniques. Polym Test 93:106878. https://doi.org/10.1016/j.polymertesting.2020.106878
35. Tardif X, Pignon B, Boyard N et al (2014) Experimental study of crystallization of PolyEtherEtherKetone (PEEK) over a large temperature range using a nano-calorimeter. Polym Test 36:10–19. https://doi.org/10.1016/j.polymertesting.2014.03.013
36. Pu J, McIlroy C, Jones A, Ashcroft I (2021) Understanding mechanical properties in fused filament fabrication of polyether ether ketone. Addit Manuf 37:101673. https://doi.org/10.1016/j.addma.2020.101673
37. He Y, Shen M, Wang Q et al (2023) Effects of FDM parameters and annealing on the mechanical and tribological properties of PEEK. Compos Struct 313:116901. https://doi.org/10.1016/j.compstruct.2023.116901
38. Regis M, Bellare A, Pascolini T, Bracco P (2017) Characterization of thermally annealed PEEK and CFR-PEEK composites: structure-properties relationships. Polym Degrad Stab 136:121–130. https://doi.org/10.1016/j.polymdegradstab.2016.12.005
39. https://www.creatbot.com/en/creatbot-peek-300.html
40. Blundell DJ, Osborn BN (1983) The morphology of poly(aryl-ether-ether-ketone). Polymer (Guildf) 24:953–958. https://doi.org/10.1016/0032-3861(83)90144-1
41. Lannunziata Erika and Giubilini A and SA and MP (2024) Influence of process parameters on compression properties of 3D printed polyether-ether-ketone by fused filament fabrication. In: Silva Francisco J. G. and Pereira AB and CRDSG (ed) Flexible Automation and Intelligent Manufacturing: Establishing Bridges for More Sustainable Manufacturing Systems. Springer Nature Switzerland, Cham, 336–344
42. Lee A, Wynn M, Quigley L et al (2022) Effect of temperature history during additive manufacturing on crystalline morphology of PEEK. Adv Ind Manuf Eng 4:100085. https://doi.org/10.1016/j.aime.2022.100085
43. Zhang J, Vasiliauskaite E, De Kuyper A et al (2022) Temperature analyses in fused filament fabrication: from filament entering the hot-end to the printed parts. 3D Print Addit Manuf 9:132–142. https://doi.org/10.1089/3dp.2020.0339
44. Jiang Z, Liu P, Sue H-J, Bremner T (2019) Effect of annealing on the viscoelastic behavior of poly(ether-ether-ketone). Polymer (Guildf) 160:231–237. https://doi.org/10.1016/j.polymer.2018.11.052
45. Arzak A, Eguiazábal JI, Nazábal J (1991) Effect of annealing on the properties of poly(ether ether ketone). Polym Eng Sci 31:586–591. https://doi.org/10.1002/pen.760310809
46. Patel P, Hull TR, Lyon RE et al (2011) Investigation of the thermal decomposition and flammability of PEEK and its carbon and glass-fibre composites. Polym Degrad Stab 96:12–22. https://doi.org/10.1016/j.polymdegradstab.2010.11.009
47. Ramgobin A, Fontaine G, Bourbigot S (2020) A case study of polyether ether ketone (I): investigating the thermal and fire behavior of a high-performance material. Polymers (Basel) 12:1789. https://doi.org/10.3390/polym12081789
48. Maqsood M, Seide G (2019) Investigation of the flammability and thermal stability of halogen-free intumescent system in biopolymer composites containing biobased carbonization agent and mechanism of their char formation. Polymers (Basel) 11:48. https://doi.org/10.3390/polym11010048
49. Mohammed AA, Al-Hassani ES, Oleiwi JK, Ghaffarian SR (2019) The effect of annealing on the behavior of polyetheretherketone composites compared to pure titanium. Mater Res Express 6:125405. https://doi.org/10.1088/2053-1591/ab5503
50. Vindokurov I, Pirogova Y, Tashkinov M, Silberschmidt VV (2022) Effect of heat treatment on elastic properties and fracture toughness of fused filament fabricated PEEK for biomedical applications. Polymers (Basel) 14:5521. https://doi.org/10.3390/polym14245521
51. Comelli CA, Davies R, van der Pol H, Ghita O (2022) PEEK filament characteristics before and after extrusion within fused filament fabrication process. J Mater Sci 57:766–788. https://doi.org/10.1007/s10853-021-06652-0
52. Comelli CA, Yi N, Davies R et al (2022) Material extrusion thermal model mapped across polyetheretherketone isothermal and continuous cooling transformation charts. Addit Manuf 59:103129. https://doi.org/10.1016/j.addma.2022.103129
53. Bellehumeur C, Li L, Sun Q, Gu P (2004) Modeling of bond formation between polymer filaments in the fused deposition modeling process. J Manuf Process 6:170–178. https://doi.org/10.1016/S1526-6125(04)70071-7
54. Yang C, Tian X, Li D et al (2017) Influence of thermal processing conditions in 3D printing on the crystallinity and mechanical properties of PEEK material. J Mater Process Technol 248:1–7. https://doi.org/10.1016/j.jmatprotec.2017.04.027
55. Pulipaka A, Gide KM, Beheshti A, Bagheri ZS (2023) Effect of 3D printing process parameters on surface and mechanical properties of FFF-printed PEEK. J Manuf Process 85:368–386. https://doi.org/10.1016/j.jmapro.2022.11.057
56. Rinaldi M, Ghidini T, Cecchini F et al (2018) Additive layer manufacturing of poly (ether ether ketone) via FDM. Compos B Eng 145:162–172. https://doi.org/10.1016/j.compositesb.2018.03.029
57. Volpini V, Giubilini A, Corsi L et al (2022) Characterization of biocompatible scaffolds manufactured by fused filament fabrication of poly(3-hydroxybutyrate-*co*-3-hydroxyhexanoate). R Soc Open Sci 9:211485. https://doi.org/10.1098/rsos.211485
58. Tseng JW, Liu CY, Yen YK, Belkner J, Bremicker T, Liu BH, Sun TJ, Wang AB (2018) Screw extrusion-based additive manufacturing of PEEK. Mater Des 140:209–221. https://doi.org/10.1016/j.matdes.2017.11.032
59. Song X, Shi D, Song P, Han X, Wei Q, Huang C (2021) Fused deposition modeling of poly(ether ether ketone) scaffolds. High Temp Mater Process 40:1–11. https://doi.org/10.1515/htmp-2021-0009
60. Wang Y, Müller WD, Rumjahn A, Schmidt F, Schwitalla AD (2021) Mechanical properties of fused filament fabricated PEEK for biomedical applications depending on additive manufacturing parameters. J Mech Behav Biomed Mater 115: 104250. https://doi.org/10.1016/j.jmbbm.2020.104250
61. Qin W, Li Y, Ma J, Liang Q, Tang B (2019) Mechanical properties and cytotoxicity of hierarchical carbon fiberreinforced poly (ether-ether-ketone) composites used as implant materials. J Mech Behav Biomed Mater 89:227–233. https://doi.org/10.1016/j.jmbbm.2018.09.040
62. Fontana L, Giubilini A, Arrigo R et al (2022) Characterization of 3D printed polylactic acid by fused granular fabrication through printing accuracy, porosity, thermal and mechanical analyses. Polymers (Basel) 14:3530. https://doi.org/10.3390/polym14173530
63. Vidakis N, Petousis M, Mountakis N, Karapidakis E (2023) Box-Behnken modeling to quantify the impact of control parameters

on the energy and tensile efficiency of PEEK in MEX 3D-printing. Heliyon 9:e18363. https://doi.org/10.1016/j.heliyon.2023.e18363
64. Kim K, Noh H, Park K et al (2022) Characterization of power demand and energy consumption for fused filament fabrication using CFR-PEEK. Rapid Prototyp J 28:1394–1406. https://doi.org/10.1108/RPJ-07-2021-0188
65. Hassan MR, Jeon HW, Kim G, Park K (2021) The effects of infill patterns and infill percentages on energy consumption in fused filament fabrication using CFR-PEEK. Rapid Prototyp J 27:1886–1899. https://doi.org/10.1108/RPJ-11-2020-0288

Publisher's Note Springer Nature remains neutral with regard to jurisdictional claims in published maps and institutional affiliations.